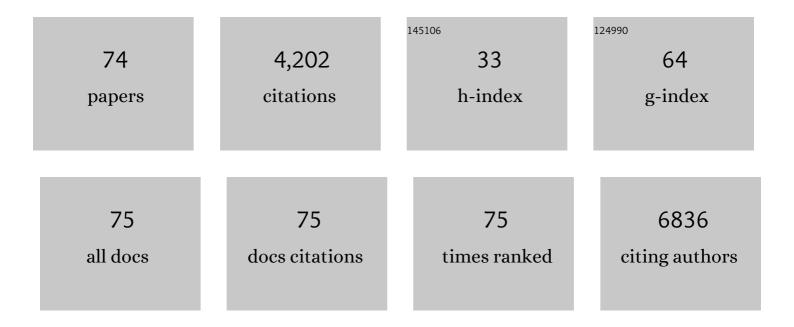
## Yabo Wang

List of Publications by Year in descending order

Source: https://exaly.com/author-pdf/1880913/publications.pdf Version: 2024-02-01



YARO WANC

#	Article	IF	CITATIONS
1	Bioleaching assisted conversion of refractory low-grade ferruginous rhodochrosite to Mn-Fe based catalysts for sulfathiazole degradation. Chemical Engineering Journal, 2022, 427, 130804.	6.6	4
2	Fe2P/biocarbon composite derived from a phosphorus-containing biomass for levofloxacin removal through peroxymonosulfate activation. Chemical Engineering Journal, 2022, 427, 130928.	6.6	22
3	Efficient removal of uranium in aqueous solution by Al-doped hydroxyapatite: Static/dynamic adsorption behaviors and mechanism study. Environmental Technology and Innovation, 2022, 25, 102103.	3.0	25
4	Ni2P/biocarbon composite derived from an unusual phosphorus-rich precursor as a superior catalyst for 4-nitrophenol reduction. Chemical Engineering Journal Advances, 2022, 9, 100238.	2.4	6
5	Tributyl phosphate degradation and phosphorus immobilization by MnO2: Reaction condition optimization and mechanism exploration. Journal of Hazardous Materials, 2022, 432, 128725.	6.5	9
6	Photocatalytic removal of sulfamethoxazole using yeast biomass-derived NixP/biocarbon composites in the presence of dye sensitizer. Journal of Environmental Chemical Engineering, 2022, 10, 107426.	3.3	4
7	Photochemical degradation of chloramphenicol over jarosite/oxalate system: Performance and mechanism investigation. Journal of Environmental Chemical Engineering, 2021, 9, 104570.	3.3	9
8	Yeast biomass-induced Co2P/biochar composite for sulfonamide antibiotics degradation through peroxymonosulfate activation. Environmental Pollution, 2021, 268, 115930.	3.7	65
9	Co-pyrolysis of spent radioactive ion exchange resin and manganese dioxide: Decrease the decomposition temperatures of functional groups. Journal of Hazardous Materials, 2021, 418, 126275.	6.5	17
10	Technical framework for wastewater-based epidemiology of SARS-CoV-2. Science of the Total Environment, 2021, 791, 148271.	3.9	18
11	Shape-controllable synthesis of MnO <sub>2</sub> nanostructures from manganese-contained wastewater for phenol degradation by activating peroxymonosulphate: performance and mechanism. Environmental Technology (United Kingdom), 2020, 41, 2037-2048.	1.2	12
12	Enhanced Cr(VI) removal by waste biomass derived nitrogen/oxygen co-doped microporous biocarbon. Environmental Science and Pollution Research, 2020, 27, 5433-5445.	2.7	6
13	Hydrothermal route-enabled synthesis of sludge-derived carbon with oxygen functional groups for bisphenol A degradation through activation of peroxymonosulfate. Journal of Hazardous Materials, 2020, 388, 121801.	6.5	64
14	In situ transesterification of wet sewage sludge via hydrothermal process: Biodiesel production and residue utilization. Biomass and Bioenergy, 2020, 141, 105715.	2.9	9
15	FexP/biochar composites induced oxygen-driven Fenton-like reaction for sulfamethoxazole removal: Performance and reaction mechanism. Chemical Engineering Journal, 2020, 396, 125321.	6.6	43
16	Dual-templated 3D nitrogen-enriched hierarchical porous carbon aerogels with interconnected carbon nanosheets from self-assembly natural biopolymer gel for supercapacitors. Electrochimica Acta, 2020, 353, 136514.	2.6	34
17	A novel g-C3N4 modified biosynthetic Fe(III)-hydroxysulfate for efficient photoreduction of Cr(VI) in wastewater treatment under visible light irradiation. Chemical Engineering Journal, 2020, 398, 125632.	6.6	28
18	Sustainable production of nano α-Fe2O3/N-doped biochar hybrid nanosheets for supercapacitors. Sustainable Energy and Fuels, 2020, 4, 4522-4530.	2.5	17

YABO WANG

#	Article	IF	CITATIONS
19	Development of metal sulfide–based photocatalysts for hydrogen evolution under visible light. , 2020, , 369-384.		4
20	Molten salt induced nitrogen-doped biochar nanosheets as highly efficient peroxymonosulfate catalyst for organic pollutant degradation. Environmental Pollution, 2020, 260, 114053.	3.7	60
21	Direct conversion of wet sewage sludge to carbon catalyst for sulfamethoxazole degradation through peroxymonosulfate activation. Science of the Total Environment, 2020, 728, 138853.	3.9	24
22	A bifunctional CoP/N-doped porous carbon composite derived from a single source precursor for bisphenol A removal. RSC Advances, 2020, 10, 9976-9984.	1.7	15
23	One-pot hydrothermal synthesis of micaceous iron oxide pigment from jarosite waste. Journal of Coatings Technology Research, 2019, 16, 213-220.	1.2	6
24	Phosphorus-rich microorganism-enabled synthesis of cobalt phosphide/carbon composite for bisphenol A degradation through activation of peroxymonosulfate. Chemical Engineering Journal, 2019, 378, 122187.	6.6	49
25	Facile synthesis of a magnetic chlorapatite composite with a high efficiency and recyclable adsorption for Congo red. Materials Research Express, 2019, 6, 116118.	0.8	0
26	Molten salt and air induced nitrogen-containing graphitic hierarchical porous biocarbon nanosheets derived from kitchen waste hydrolysis residue for energy storage. Journal of Power Sources, 2019, 439, 227096.	4.0	42
27	One-step synthesis of nitrogen-doped sludge carbon as a bifunctional material for the adsorption and catalytic oxidation of organic pollutants. Science of the Total Environment, 2019, 680, 51-60.	3.9	83
28	An adsorbent based on humic acid and carboxymethyl cellulose for efficient dye removal from aqueous solution. International Journal of Biological Macromolecules, 2019, 135, 790-797.	3.6	24
29	Iron-rich microorganism-enabled synthesis of magnetic biocarbon for efficient adsorption of diclofenac from aqueous solution. Bioresource Technology, 2019, 282, 310-317.	4.8	55
30	Cobalt oxide loaded graphitic carbon nitride as adsorptive photocatalyst for tetracycline removal from aqueous solution. Chemosphere, 2019, 218, 169-178.	4.2	33
31	Preparation of temperature-sensitive Xanthan/NIPA hydrogel using citric acid as crosslinking agent for bisphenol A adsorption. Carbohydrate Polymers, 2019, 206, 94-101.	5.1	36
32	Cobaltâ€doped biogenic manganese oxides for enhanced tetracycline degradation by activation of peroxymonosulfate. Journal of Chemical Technology and Biotechnology, 2019, 94, 752-760.	1.6	34
33	Utilization of Waste Biomass (Kitchen Waste) Hydrolysis Residue as Adsorbent for Dye Removal: Kinetic, Equilibrium, and Thermodynamic Studies. Applied Biochemistry and Biotechnology, 2018, 185, 971-985.	1.4	10
34	Ultrasonic-enhanced Fenton-like degradation of bisphenol A using a bio-synthesized schwertmannite catalyst. Journal of Hazardous Materials, 2018, 344, 689-697.	6.5	69
35	Synthesis and characterization of CuFeMnO4 prepared by co-precipitation method. Journal of Materials Science, 2018, 53, 3581-3589.	1.7	20
36	Thermally treated fungal manganese oxides for bisphenol A degradation using sulfate radicals. Chemical Engineering Journal, 2018, 335, 728-736.	6.6	77

YABO WANG

#	Article	IF	CITATIONS
37	Nearly Pure Red Color Upconversion Luminescence of Ln-Doped Sc <sub>2</sub> O <sub>3</sub> with Unexpected RE-MOFs Molecular Alloys as Precursor. Inorganic Chemistry, 2018, 57, 10511-10517.	1.9	8
38	A new approach for excess sludge reduction by manganese dioxide oxidation: performance, kinetics, and mechanism studies. Environmental Science and Pollution Research, 2018, 25, 29356-29365.	2.7	13
39	Bioconversion of Welan Gum from Kitchen Waste by a Two-Step Enzymatic Hydrolysis Pretreatment. Applied Biochemistry and Biotechnology, 2017, 183, 820-832.	1.4	11
40	CdS nanoparticles loaded on porous poly-melamine–formaldehyde polymer for photocatalytic dye degradation. Research on Chemical Intermediates, 2017, 43, 5083-5090.	1.3	8
41	Enzymatic treatment on cotton fibers: degradation kinetics of pectin and influence of shape change on adsorption. Fibers and Polymers, 2017, 18, 1882-1890.	1.1	2
42	Effect of pretreatment on the enzymatic hydrolysis of kitchen waste for xanthan production. Bioresource Technology, 2017, 223, 84-90.	4.8	64
43	Anionic polymer as a quasi-neutral medium for low-cost synthesis of titanosilicate molecular sieves in the presence of high-concentration alkali metal ions. Journal of Catalysis, 2016, 338, 321-328.	3.1	18
44	Municipal solid waste incineration bottom ash supported cobalt oxide catalysts for dye degradation using sulfate radical. Journal of the Taiwan Institute of Chemical Engineers, 2016, 68, 246-253.	2.7	11
45	Molybdenum carbide microcrystals: Efficient and stable catalyst for photocatalytic H2 evolution from water in the presence of dye sensitizer. Journal of Materiomics, 2016, 2, 344-349.	2.8	8
46	Anionic and cationic dyes adsorption on porous poly-melamine-formaldehyde polymer. Chemical Engineering Research and Design, 2016, 114, 258-267.	2.7	72
47	Conversion of municipal solid waste incineration bottom ash to sorbent material: Effect of ash particle size. Journal of the Taiwan Institute of Chemical Engineers, 2016, 68, 351-359.	2.7	14
48	Biosynthesis of xanthan gum by Xanthomonas campestris LRELP-1 using kitchen waste as the sole substrate. Carbohydrate Polymers, 2016, 151, 684-691.	5.1	96
49	Conversion of municipal solid waste incineration bottom ash to sorbent material for pollutants removal from water. Journal of the Taiwan Institute of Chemical Engineers, 2016, 60, 275-286.	2.7	23
50	Cation-exchange resin towards low-cost synthesis of high-performance TS-1 zeolites in the presence of alkali-metal ions. RSC Advances, 2016, 6, 15615-15621.	1.7	5
51	CdS quantum dots and tungsten carbide supported on anatase–rutile composite TiO <sub>2</sub> for highly efficient visible-light-driven photocatalytic H <sub>2</sub> evolution from water. Catalysis Science and Technology, 2016, 6, 2206-2213.	2.1	62
52	Photocatalytic Reduction of Carbon Dioxide over Selfâ€Assembled Carbon Nitride and Layered Double Hydroxide: The Role of Carbon Dioxide Enrichment. ChemCatChem, 2014, 6, 2315-2321.	1.8	130
53	Surface Modification of Pollen-Shape Carriers for Dry Powder Inhalation through Surface Etching. Industrial & Engineering Chemistry Research, 2014, 53, 19943-19950.	1.8	4
54	Post-synthesis modification of a metal–organic framework to construct a bifunctional photocatalyst for hydrogen production. Energy and Environmental Science, 2013, 6, 3229.	15.6	336

YABO WANG

#	Article	IF	CITATIONS
55	Immobilizing CdS quantum dots and dendritic Pt nanocrystals on thiolated graphene nanosheets toward highly efficient photocatalytic H2 evolution. Nanoscale, 2013, 5, 9830.	2.8	110
56	Nobleâ€Metalâ€Free NiS/C <sub>3</sub> N <sub>4</sub> for Efficient Photocatalytic Hydrogen Evolution from Water. ChemSusChem, 2013, 6, 2263-2268.	3.6	289
57	Carbon nitride nanosheets for photocatalytic hydrogen evolution: remarkably enhanced activity by dye sensitization. Catalysis Science and Technology, 2013, 3, 1703.	2.1	225
58	Photochemical Deposition of Pt on CdS for H <sub>2</sub> Evolution from Water: Markedly Enhanced Activity by Controlling Pt Reduction Environment. Journal of Physical Chemistry C, 2013, 117, 783-790.	1.5	178
59	Formation of Sn@C Yolk–Shell Nanospheres and Core–Sheath Nanowires for Highly Reversible Lithium Storage. Particle and Particle Systems Characterization, 2013, 30, 873-880.	1.2	43
60	Carbon Nanospheres—A Dark Support for Effective Loading of Pt Catalyst and Protection of Dye Sensitizer in Photocatalytic Hydrogen Evolution. Science of Advanced Materials, 2013, 5, 1658-1666.	0.1	2
61	Formation of 1D Hierarchical Structures Composed of Ni <sub>3</sub> S <sub>2</sub> Nanosheets on CNTs Backbone for Supercapacitors and Photocatalytic H <sub>2</sub> Production. Advanced Energy Materials, 2012, 2, 1497-1502.	10.2	321
62	Ni <sup>2+</sup> -doped Zn <sub>x</sub> Cd <sub>1â^'x</sub> S photocatalysts from single-source precursors for efficient solar hydrogen production under visible light irradiation. Catalysis Science and Technology, 2012, 2, 581-588.	2.1	66
63	Low-Cost Carbon Nanospheres for Efficient Removal of Organic Dyes from Aqueous Solutions. Industrial & Engineering Chemistry Research, 2012, 51, 13438-13444.	1.8	39
64	Cobalt Phosphate–ZnO Composite Photocatalysts for Oxygen Evolution from Photocatalytic Water Oxidation. Industrial & Engineering Chemistry Research, 2012, 51, 9945-9951.	1.8	71
65	Highly active ZnxCd1â^'xS photocatalysts containing earth abundant elements only for H2 production from water under visible light. Catalysis Science and Technology, 2011, 1, 940.	2.1	80
66	Self-assembled dye–layered double hydroxide–Pt nanoparticles: a novel H2 evolution system with remarkably enhanced stability. Nanoscale, 2011, 3, 4655.	2.8	32
67	Synthesis of Zn–Cu–Cd sulfide nanospheres with controlled copper locations and their effects on photocatalytic activities for H2 production. International Journal of Hydrogen Energy, 2010, 35, 5245-5253.	3.8	26
68	Chitosan membranes filled by GPTMS-modified zeolite beta particles with low methanol permeability for DMFC. Chemical Engineering and Processing: Process Intensification, 2010, 49, 278-285.	1.8	37
69	Highly efficient and noble metal-free NiS/CdS photocatalysts for H2 evolution from lactic acid sacrificial solution under visible light. Chemical Communications, 2010, 46, 7631.	2.2	450
70	Photocatalytic properties of porous C-doped TiO2 and Ag/C-doped TiO2 nanomaterials by eggshell membrane templating. Journal of Nanoparticle Research, 2009, 11, 375-384.	0.8	39
71	Proton conducting CS/P(AA-AMPS) membrane with reduced methanol permeability for DMFCs. Journal of Power Sources, 2008, 180, 143-153.	4.0	87
72	Zeolite beta-filled chitosan membrane with low methanol permeability for direct methanol fuel cell. Journal of Power Sources, 2008, 183, 454-463.	4.0	87

#	Article	IF	CITATIONS
73	Carbon-modified TiO2 nanotubes with enhanced photocatalytic activity synthesized by a facile wet chemistry method. Scripta Materialia, 2008, 59, 352-355.	2.6	29
74	Synthesis of anatase titania-carbon nanotubes nanocomposites with enhanced photocatalytic activity through a nanocoating-hydrothermal process. Journal of Nanoparticle Research, 2007, 9, 1087-1096.	0.8	72